PCCP

Interaction Energy and Isosteric Heat of Adsorption between Hydrogen and Magnesium Diboride

Journal:	*Physical Chemistry Chemical Physics*
Manuscript ID	CP-ART-10-2022-004730.R1
Article Type:	Paper
Date Submitted by the Author:	14-Dec-2022
Complete List of Authors:	PHAM, THI Kieu Ngan; University of Hawai'i at Mānoa, Mechanical Engineering Li, Sichi; Lawrence Livermore National Laboratory, Materials Science Division Brown, Joseph; University of Hawai'i at Manoa, Mechanical Engineering

ARTICLE

Interaction Energy and Isosteric Heat of Adsorption between Hydrogen and Magnesium Diboride

Received 00th January 20xx,
Accepted 00th January 20xx

DOI: 10.1039/x0xx00000x

Thi Kieu Ngan Pham,*[a] Sichi Li,[b] and Joseph J. Brown[a]

Hydrogen storage material is a crucial research topic for future energy utilization employing hydrogen and among those of interest, magnesium diboride (MgB_2) has shown its prevalence. In this study, a first-principles analytical adsorption model of one hydrogen molecule in vicinity of various magnesium diboride crystal surfaces was developed, in order to obtain surface thermodynamic properties as functions of molecular and lattice properties. Henry's Law constant (K_H) and isosteric heat of adsorption (ΔH_{ads}) - indicators of the affinity between a gaseous molecule and a solid surface are thus calculated. The results in this paper not only address questions pertaining to the first stage of hydrogen storage processes but also advance the understanding of physisoprtion thermodynamics of a neutral molecule (H_2) coming in contact with a layered metallic-like surface (MgB_2). Although the model is built from a framework of classical calculations, quantum effects are incorporated as fractional charge of the ions on the free surfaces, which is essential for calculation of analytic thermodynamic values that approximate calculations from other methods. To benchmark our theoretical models, periodic density functional calculations were performed to determine the interactions between H_2 and different MgB_2 surfaces from first-principles. By considering both top and sublayer of MgB_2 in calculating interaction energy, we have analytically and computationally calculated the interaction energies of H_2 molecule and MgB_2's terminated planes, and witnessed the strong dependence of interaction energies to surface charges. We have also observed a dipole flipping phenomenon which explains the discontinuity seen in the interaction energy graph of Mg (0001). Both analytical and computational results showed heat of adsorption at zero coverage varying at very low range ($< 7\ kJ\ mol^{-1}$).

Introduction

The advancement of renewable technologies is a key current focus of energy research, supported by government and corporate investment and made exigent by challenges of climate change and energy security. For instance, in 2022, a 9-billion-dollar initiative was passed in the US government to increment the development of hydrogen as fuel of the future.[1] One pertinent scientific challenge is the pursuit of a practical hydrogen storage material that matches with US Department of Energy (DOE) requirements[2], which set targets of gravimetric and volumetric capacities for specified on-board systems, recommendation for ambient temperature, safe operation, etc. Fundamentally, these requirements all derive from the thermodynamics of hydrogenation and dehydrogenation reactions of a candidate hydrogen storage material.

One promising candidate material for hydrogen storage, magnesium diboride (MgB_2), has theoretically and experimentally exhibited greater than $11\ wt\%$ of hydrogen storage capacity, thereby exceeding the DOE's gravimetric requirement, and also has favorable enthalpy of hydrogen release $(38\ kJ\ mol^{-1})$ but experimental conditions for these observations remained extreme.[3–6] This material poses a fundamental question regarding the mechanism of hydrogen gaseous molecules coming in contact with MgB_2 and its interaction energy at ambient temperature. The MgB_2 structure has alternating layers of closed-packed trigonal magnesium and honeycomb-like lattice of boron, featuring a hexagonal crystal structure with lattice constants being: $a = 3.074$ Å and $c = 3.518$ Å.[7] Figure 1 displays the crystal structure of pristine MgB_2. Even though MgB_2 has a metallic nature, the interaction of H_2 molecules and MgB_2 can be different from the already well-developed knowledge about the interaction between H_2 and metals.[8,9]

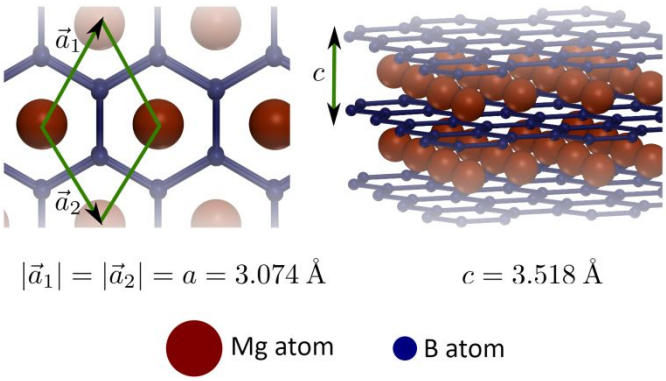

Figure 1: Atomic arrangements in a pristine MgB_2 featuring hexagonal, layered crystal structure with two lattice vectors a_1,a_2 in the (0001) plane and the gap between two identical layers being distance c.

[a] Department of Mechanical Engineering, University of Hawai'i at Mānoa, Hawai'i 96822, USA.
[b] Laboratory for Energy Applications for the Future (LEAF), Lawrence Livermore National Laboratory, Livermore, California 94550, USA.
Electronic Supplementary Information (ESI) available: See DOI: 10.1039/x0xx00000x

In prior studies using carbon-based nanomaterials for hydrogen storage, the addition of alkali/transition metals (TMs) was employed because these metals act as catalytic sites for hydrogen molecule dissociation, creating interaction between the occupied sigma orbital of hydrogen with the vacant metal *d*-orbitals or hybrid *sp* orbital at surface.[10–14] The mechanism of H_2 interaction with various metals is well-known to initiate with a physisorption step, with subsequent dissociative chemisorption where the H atoms penetrate and diffuse to the lattice.[15–18] One early theory developed by *Norskov and Houmoller* in 1981 thoroughly described the kinetic movement of H_2 molecule adsorption on Mg (metal) fcc (100) surfaces, accomplished via precursor states. The H_2 initially maintains a physisorbed state and as approaching the surface, it encounters an outer activation barrier. Passing the barrier, H_2 stays in a molecularly chemisorbed state and can freely move along the surface. It then dissociates into H atoms at energetically favorable sites.[19] In 1985, *Nakatsuji and Hada* used *ab initio* theory to show a stable molecular adsorption state of H_2 on Pd surface at 1.5 Å distance.[20] This study also witnessed a smooth equilibrium between molecular H_2 and its dissociated form. Although dissociation is the dominant case for adsorption on metals, there is no clear theoretical background on metallic heterogeneous solids, such as MgB_2.

The focus on MgB_2/$Mg(BH)_4$ as well as borohydrides for hydrogen storage has been discussed elsewhere with the key advantage being the potential for high gravimetric and volumetric storage densities as noted above.[6,21–25] For hydrogen storage purposes, the interaction between hydrogen with an ideal sorbent material can be intuitively understood to have an optimal range (reportedly $\sim 15-48\ kJ\ mol^{-1}$ by *Prayogo et. al*)[26], where it is larger than physical adsorption for better retention at room temperature and smaller than chemisorption in order to allow low energy desorption.[27] A study from Ray *et al.* in 2017 showed a direct hydrogenation from MgB_2 to $Mg(BH)_4$, , which went through two steps: (1) dissociation of the H_2 molecule and (2) diffusive absorption initially from the high energy B-B bond.[21] This could be attributed to the electron tunneling of the occupied hydrogen orbitals and a suitable surface plane's electron wave functions.[18] Among the recent research on MgB_2 for hydrogen storage, exclusive study into the dissociated state and H-atom diffusion into lattice mechanism dominates;[21–25,27,28] yet the very initial physisorbed state has only been vaguely discussed. The dissociation enables better hydrogen storage capacity and at the same time, makes it thermodynamically more expensive to desorb these H_2. The first stage of hydrogen storage, in which H_2 gas remains in its molecule form, is thus important because we expect the adsorption energy here to fall within the optimal range discussed above. Studying singular gas adsorption on a layered material like MgB_2 is also of current interest because this group of material, despite in its 3D form, shows 1D and 2D properties in the perpendicular and lateral directions of the layers, respectively.[29] Magnesium diboride is fundamentally interesting in the study of layered materials because it is a heterogeneous layered material. The interface between adjacent layers is atomically thick and exhibits metallic interaction. The in-plane and inter-plane distances between two B atoms are different. This leads to anisotropy in mechanical, thermal and electronic properties of this material. With the chemical structure MgB_2, Mg is nominally understood to have valence charge of $2+$. However, it was previously observed that there is back charge transfer from B to Mg which means MgB_2 is not fully ionized.[30–32] More interestingly, the charge values of individual atoms on each plane also vary with terminated planes and their sublayers. It is thus appealing to examine gas adsorption on different terminated planes of a layered material. Computational tools are specifically powerful in this case to identify charge density on a plane. Meanwhile, interaction energy between a gaseous molecule and a solid surface is a complex integration of many factors: sorbate and sorbent electronic properties, sorbent's crystal structure, the distance between the two, and the surrounding environment, which can be considered as vacuum for this study. Steele set a foundation for analytical representation of gas-solid interactions, which played a crucial role in modern interface science, yet the studied sorbent was limited to graphite. [33] The opportunity then presents itself to develop a model for more complex materials such as a metal-like layered ++++sorbent like MgB_2. Having an analytical theory can clarify the important factors contributing to the calculated interaction energy. Surface charge effects can be examined here through a sensitivity analysis to establish their importance to the overall interaction energy. With a formulated approach, future studies may be able to expand the theory to incorporate other effects such as intercalation into layered materials, depending on the charges of intercalant. Intercalation is a known process that enables dramatic charge transfer between the layers.[29] Such a study can also pave the way for strategies to improve hydrogen storage capacity by manipulating contributing factors in the analytical representation.

In this paper, an analytical model of H_2 adsorption on MgB_2 at different terminated planes was developed. The interaction energies at different terminated planes and varying charge values were calculated. We performed our study at ambient temperature, which is a crucial factor in choosing H_2 storage material because hydrogen uptake at room temperature creates ease of activation, maintain H_2 cyclic stability and cycle life.[34] From the model, a thermodynamic property – the isosteric heat of adsorption at zero coverage was also calculated. Computationally identified surface charges of MgB_2 using density functional theory (DFT) are also presented and incorporated as ion charge inputs to the adsorption analytical theory.[35] To validate our adsorption analysis, we performed DFT calculations at the SCAN-rVV10 level of theory to explicitly determine the binding energies of H_2 to the different MgB_2 surfaces that we explored.

Theory

Within the adsorption medium, a H_2 gaseous molecule can arbitrarily approach a terminated surface plane of MgB_2 to the point of physisorption. A surface plane of MgB_2 comprises multiple lattice unit cells, and the positions of atoms in each unit cell repeat throughout the surface. As one H_2 gaseous molecule translates in x-y direction (in-plane), the total interaction energy ($u_s(r)$) between one H_2 and the MgB_2 surface plane can be described as a periodic function represented via Fourier series:

$$u_s(r) = \sum_g w_g(z) \exp\left(i\vec{g}\cdot\vec{\tau}\right) \quad (1)$$

where $\vec{g} = 2\pi(g_1\overrightarrow{b_1} + g_2\overrightarrow{b_2})$ is the multiple of reciprocal lattice vectors, $\vec{\tau} = s_1\overrightarrow{a_1} + s_2\overrightarrow{a_2}$ is the two-dimensional translation vector, w_g is the Fourier coefficient, $\left|\overrightarrow{b_1}\right| = \left|\overrightarrow{b_2}\right| = \frac{\csc\theta}{\left|\overrightarrow{a_1}\right|}$, θ is the angle between two lattice vectors $\overrightarrow{a_1}$ and $\overrightarrow{a_2}$, (s_1,s_2) are coordinates of the H_2 adsorption sites in the unit lattice cell.

This total interaction energy $u_s(r)$ can also be understood as the summation of single interactions between the H_2 molecule and each atom on the solid's surface. The single interaction discussed in this

study (H_2 – MgB_2) includes the dispersion-repulsion interaction which can be represented through the Lennard-Jones 12-6 model (Eq. 2), termed as the "fluctuating dipole interaction", and the ion-induced dipole interaction (Eq. 3), termed as the "induced dipole interaction".

$$e_{gs} = 4\varepsilon_{gs}\left\{\left(\frac{\sigma_{gs}}{r_{ij}}\right)^{12} - \left(\frac{\sigma_{gs}}{r_{ij}}\right)^{6}\right\} \quad (2)$$

where $e_{gs}\,(kJ\,mol^{-1})$ is the Lennard-Jones 12-6 interaction energy, $\varepsilon_{gs}\,(kJ\,mol^{-1}) = \sqrt{\varepsilon_{MgB_2}\varepsilon_{H_2}}$ is the potential well depth, $\sigma_{gs} = \frac{\sigma_{MgB_2} + \sigma_{H_2}}{2}$ (m) is the distance at which the interaction energy equal zero, $r_{ij}\,(m)$ is the distance between two entities. The term $\sigma_{MgB_2}$was taken as the bonding length between two atoms on a lattice plane of MgB_2. The ε_{MgB_2} term was taken as $0.4\ kJ\ mol^{-1}$ for B planes[36] and $0.46\ kJ\ mol^{-1}$ for Mg plane.[37]

$$\phi_{Ind} = \frac{-\alpha q^2}{2r^4(4\pi\varepsilon_0)^2} \quad (3)$$

where $\phi_{Ind}\,(kJ\,mol^{-1})$ is the induction energy, $\alpha\,(C^2\,m\,N^{-1})$ is the H_2 polarizability, $q\,(C)$ is the charge of each atom on the solid surface, ε_0 $(C^2\,m^{-2}\,N^{-1})$ is the vacuum permittivity. In this study, the charges of Mg and B are calculated with DFT using the Bader formalism.[38–41] Based on equation (1), (2) and (3), the total interaction energy of one H_2 molecule at a distance $z\,(m)$ from a surface can be illustrated as below:

$$u_s(r_i) = \sum_j (e_{gs}(r_{ij}) + \phi_{Ind}) \quad (4)$$
$$= \sum_{l_1,l_2}\sum_k \left[e_{gs}(z_\alpha, \vec{\tau} + \vec{l} + \overrightarrow{m_k}) + \emptyset_{Ind}(z_\alpha, \vec{\tau} + \vec{l} + \overrightarrow{m_k})\right]$$

From equation (1), the Fourier series coefficient w_g can be displayed as:

$$w_g(z_\alpha) = \frac{1}{a_s}\int \exp(-i\vec{g}\cdot\vec{\tau})u_s(z_\alpha, \boldsymbol{\tau})d\boldsymbol{\tau} \quad (5)$$

Combining equation (4) and (5), we have:

$$w_g(z_\alpha) = \frac{1}{a_s}\sum_k \exp(-i\vec{g}\cdot\overrightarrow{m_k})\int \exp(-i\vec{g}\cdot\vec{\tau})\left[e_{gs}(z_\alpha, \vec{\tau} + \vec{l} + \overrightarrow{m_k}) + \emptyset_{Ind}(z_\alpha\right. \quad (6)$$

$$w_g(z_\alpha) = \frac{2\pi}{a_s}\sum_k \exp\left(-i\vec{g}\cdot\overrightarrow{m_k}\right)\int_0^\infty J_0(gt)e_{gs}(r)tdt + \frac{2\pi}{a_s}\sum_k \exp(-i\vec{g}\cdot\overrightarrow{m_k})\int_0^\infty J_0(gt)\,\emptyset_{Ind}(r)tdt \quad (7)$$

It is also known according to Bessel function identities that:

$$\int_0^\infty J_0(gt)\left(\frac{1}{z^2+t^2}\right)^{n+1}tdt = \frac{1}{n!}\left(\frac{g}{2z}\right)^n K_n(gz) \quad (8)$$

$$\lim_{g\to 0}\frac{1}{n!}\left(\frac{g}{2z}\right)^n K_n(gz) = \frac{1}{2nz^{2n}},\ \ n>0 \quad (9)$$

where J_0 is the Bessel function of the first kind, of zeroth order. Plugging equation (8) and (9) into equation (7), we can obtain the fluctuating dipole interaction energy and induced dipole interaction energy from the first and second terms in Fourier series coefficient w_g in equation (7), respectively.

$$\frac{u_{fluctuating}(r)}{\varepsilon_{gs}} = \frac{2\pi}{a_s}\sum_\alpha\left\{N\left(\frac{2\sigma_{gs}^{12}}{5z_\alpha^{10}} - \frac{\sigma_{gs}^6}{z_\alpha^4}\right) + \sum_{g\neq 0}\sum_{k=1}^{N}\exp(-i\vec{g}\cdot[\overrightarrow{m_k} \quad (10)$$

$$u_{induced} = \frac{2\pi}{a_s}\sum_\alpha\left\{N\frac{C}{2z^2} + \sum_{g\neq 0}\sum_{k=1}^{N}\exp(-i\vec{g}\cdot[\overrightarrow{m_k} + \vec{\tau}]) \times (C\frac{g}{2z}K \quad (11)$$

where $a_s(m^2)$ is the unit lattice cell area, N is the number of atoms in each unit lattice cell and $C = \frac{-\alpha q^2}{2(4\pi\varepsilon_0)^2}\,(J\,m^4)$

In this analytical model, both the top layer and one sublayer are considered. MgB_2 was evaluated at 5 types of terminated planes: B-terminated (0001), Mg-terminated $(000\bar{1})$, B-terminated $(10\bar{1}0)$, Mg-terminated $(10\bar{1}0)$, and Mg-B $(11\bar{2}0)$, along with their sublayers, as listed in Table 1. Visual display of these planes and their sublayers are presented in Figure 2. Because of the consideration of sublayer, the use of singular electrostatic interaction energy between one nonpolar molecule and an ionic surface as in equation (3) is not sufficient. The coefficient C in equation (11) should involve charges of atoms of top layer and its subsequent sublayer. Distances of the two planes to the H_2 molecules should be reflect here too.

Fluctuating dipole interaction energy is the summation of interaction between H_2 and each atom on MgB_2 surface, without consideration of charge. However, for the induced dipole interaction energy, this requires further elucidation. To illustrate for the electrostatic interaction energy in regard of heterogenous charges within the surface layer and sublayer, we review one example of the B-terminated (0001) plane (sublayer: Mg-terminated $(000\bar{1})$ plane).

B_1 and B_2 negative charges exert an electric field on the H_2 nonpolar molecule that polarizes the H_2 molecule.

$$\overrightarrow{E_1} = \frac{1}{4\pi\varepsilon_0 r_1^2}\frac{q_B}{r_1}\hat{} \quad (12)$$

$$\overrightarrow{E_2} = \frac{1}{4\pi\varepsilon_0 r_2^2}\frac{q_B}{r_2}\hat{} \quad (13)$$

$$\overrightarrow{p_1} = \alpha\overrightarrow{E_1} = \frac{\alpha\ q_B}{4\pi\varepsilon_0 r_1^2}\hat{r_1} \quad (14)$$

$$\overrightarrow{p_2} = \alpha\overrightarrow{E_2} = \frac{\alpha\ q_B}{4\pi\varepsilon_0 r_2^2}\hat{r_2} \quad (15)$$

Respectively, the Mg positive charge exerts an electric field on the H_2 molecule that polarizes the H_2 molecule.

$$\overrightarrow{E_3} = \frac{1}{4\pi\varepsilon_0\ r_3^2}\frac{q_{Mg}}{r_3}\hat{} \quad (16)$$

$$\overrightarrow{p_3} = \alpha\overrightarrow{E_3} = \frac{\alpha\ q_{Mg}}{4\pi\varepsilon_0\ r_3^2}\hat{r_3} \quad (17)$$

where $\overrightarrow{E_1}$, $\overrightarrow{E_2}$ and $\overrightarrow{E_3}$ are electric field exerted by negative B_1, negative B_2 and positive Mg charges on H_2 molecule; $\overrightarrow{p_1}$, $\overrightarrow{p_2}$ and $\overrightarrow{p_3}$ are the respective dipole moments on H_2 molecule, $\overrightarrow{r_1}$, $\overrightarrow{r_2}$ and $\overrightarrow{r_3}$ are the distances between H_2 molecule to B_1, B_2 and Mg atom respectively. A simplified illustration of the entities' positions with respect to each other and dipoles is presented in Figure 3.

Because $r_1 = r_2$, the total dipole that two B atoms acting on the H_2 molecule is as below:

$$\overrightarrow{p_{12}} = \frac{\alpha}{4\pi\varepsilon_0}\frac{|q_B|}{r_1^2}\sqrt{2(1+\cos\varphi)}\hat{r}_{12} \quad (18)$$

where $\hat{r}_{12}$ describes the direction of the sum vector, φ is the angle between two vectors $\overrightarrow{p_1}$ and $\overrightarrow{p_2}$. The final dipole of the H_2 molecule induced by both B atoms and the Mg atom is described below

$$\overrightarrow{p_{123}} = \frac{\alpha}{4\pi\varepsilon_0}\sqrt{\frac{q_B^2}{r_1^4}2(1+\cos\varphi) + \frac{q_{Mg}^2}{r_3^4} + 2\frac{|q_B|q_{Mg}}{r_1^2 r_3^2}\sqrt{2(1+\cos\varphi)}\cos} \quad (19)$$

where θ is the angle between two vectors $\overrightarrow{p_{12}}$ and $\overrightarrow{p_3}$. This dipole creates three respective fields $\overrightarrow{E'_1}, \overrightarrow{E'_2}, \overrightarrow{E'_3}$ on charge q_{B1}, q_{B2} and q_{Mg}.

$$\overrightarrow{E'_1} = \overrightarrow{E'_2} = \frac{1}{4\pi\varepsilon_0}\frac{2\overrightarrow{p_{123}}}{r_1^3} \quad (20)$$

$$\overrightarrow{E'_3} = \frac{1}{4\pi\varepsilon_0}\frac{2\overrightarrow{p_{123}}}{r_3^3} \quad (21)$$

Here, $r_3 = d \times r_1 = d \times r_2$

Table 1: List of 6 terminated top planes of MgB_2 and their sublayers that are considered in the analytical model.

	Terminated Surface Plane	Sublayer(s)
5 types of terminated planes	B-terminated (0001)	Mg (0001)
	Mg-terminated $(000\bar{1})$	B (0001)
	B-terminated $(10\bar{1}0)$ (average of the two B planes)	Mg $(10\bar{1}0)$
	Mg-terminated $(10\bar{1}0)$	Average of the two B $(10\bar{1}0)$planes
	Mg-B-terminated $(11\bar{2}0)$	itself

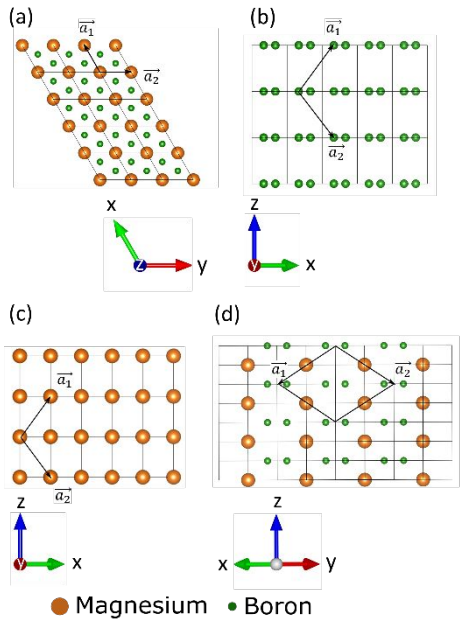

Figure 2: Top view of the 5 terminated planes of MgB_2. (a) B-terminated and Mg-terminated (0001) planes (b) B-terminated $(10\bar{1}0)$ plane (c) Mg-terminated $(10\bar{1}0)$ plane and (d) the Mg-B $(11\bar{2}0)$ plane.

ARTICLE

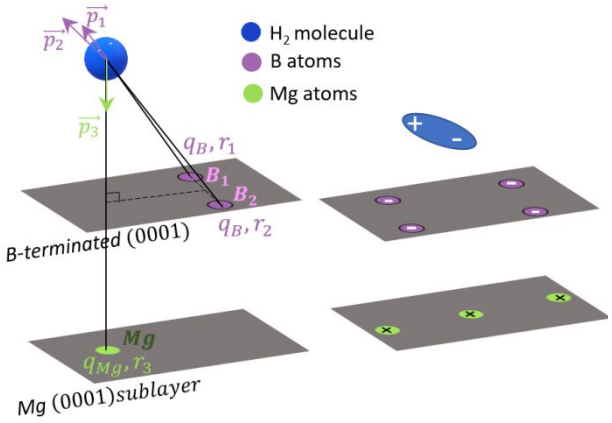

Figure 3: Illustration of the positions of H_2 molecules in respect to Mg and B atoms on the sorbent layers, with r being the distance between two entities and $\vec{p}$ being the dipole.

These fields exert respective forces on the three charges

$$\overrightarrow{F_1} = \overrightarrow{F_2} = q_B \times \overrightarrow{E_1'} = \left(\frac{1}{4\pi\varepsilon_0}\right)^2 \frac{2\alpha q_B}{r_1^3} \sqrt{\frac{q_B^2}{r_1^4} 2(1+\cos\varphi) + \frac{q_{Mg}^2}{d^4} + 2\frac{|q_B| q_{Mg}}{r_1^4 d^4}\sqrt{2(1+\cos} \quad (22)$$

$$= \left(\frac{1}{4\pi\varepsilon_0}\right)^2 \frac{2\alpha q_B}{r_1^5} \sqrt{\frac{q_B^2 2(1+\cos\varphi)}{} + \frac{q_{Mg}^2}{d^4} + 2\frac{|q_B| q_{Mg}}{d^4}\sqrt{2(1+\cos\varphi)}\cos\theta}$$

$$\overrightarrow{F_3} = q_{Mg} \times \overrightarrow{E_3'} = \left(\frac{1}{4\pi\varepsilon_0}\right)^2 \frac{2\alpha q_{Mg}}{r_3^5} \sqrt{q_B^2 2d^4(1+\cos\varphi) + q_{Mg}^2 + 2d^2|q_B| q_{Mg}\sqrt{2(1+\cos} \quad (23)$$

The interaction energy between H_2 molecule with these three charges are described below:

$$E = \int F\, dr$$

$$E_1 = E_2 \quad (24)$$

$$= -\left(\frac{1}{4\pi\varepsilon_0}\right)^2 \frac{\alpha q_B}{2r_1^4} \sqrt{\frac{q_B^2 2(1+\cos\varphi)}{} + \frac{q_{Mg}^2}{d^4} + 2\frac{|q_B| q_{Mg}}{d^4}\sqrt{2(1+\cos\varphi)}\cos\theta}$$

$$E_3 = -\left(\frac{1}{4\pi\varepsilon_0}\right)^2 \frac{2\alpha q_{Mg}}{2r_3^4} \sqrt{\frac{q_B^2 2d^4(1+\cos\varphi) + q_{Mg}^2}{+2d^2|q_B| q_{Mg}\sqrt{2(1+\cos\varphi)}\cos\theta}} \quad (25)$$

As distance between H_2 and MgB_2 planes change, there is a possibility that the direction of dipole is flipping, as shown in Figure 4, because it is a vector addition between $\overrightarrow{p_{12}}$ and $\overrightarrow{p_3}$. With that said, in case (A) where $p_{12}^2 - (p_3^2 + p_{123}^2)$ is negative (the dipole has its negative head closer to the solid plane), $E_{specific} = E_1 + E_2 + E_3$. Conversely, as in case (B) where $p_{12}^2 - (p_3^2 + p_{123}^2)$ is positive (the dipole has its positive head closer to the solid plane), $E_{specific} = -(E_1 + E_2 + E_3)$. It is often more convenient to describe equations (10), (11) in terms of lattice vectors $\overrightarrow{a_1}$, $\overrightarrow{a_2}$ and dimensionless parameters rather than Cartesian coordinates: $a_s^* = \frac{a_s}{a_1^2}$; $z^* = \frac{z}{a_1}$; $g^* = g a_1$; $A = \frac{\sigma_{gs}}{a_1}$

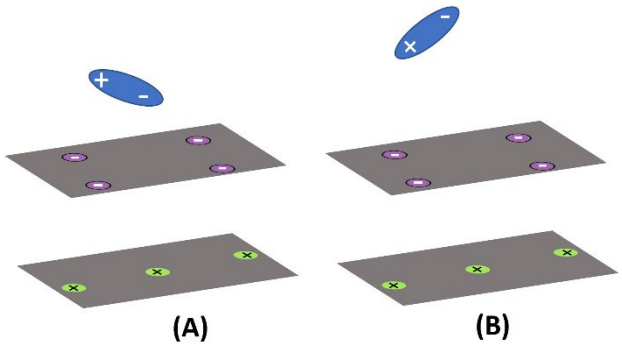

Figure 4: Illustration of the possibility of witnessing H_2 molecule dipole flipping as the distance between H_2 and MgB_2 plane changes.

$$u_s^* = \frac{u_s(r)}{\varepsilon_{gs}} = \varepsilon_{gs} \times [E_{0_{non-specific}}(z^*) + \sum_{n>0} E_{n_{non-specific}}(z^*) f_n(s_1 s_2)] \quad (26)$$

$$E_{0_{non-specific}}(z^*) = \frac{2\pi A^6 q}{a_s^*} \sum_{p=0}^{\infty} \left(\frac{2A^6}{5(z^* + p\Delta z^*)^{10}} - \frac{1}{(z^* + p\Delta z^*)^4}\right) \quad (27)$$

$$E_{n_{non-specific}}(z^*) = \frac{2\pi A^6 q}{a_s^*} \left[\frac{A^6}{30}\left(\frac{g_n^*}{2z^*}\right)^5 K_5(g_n^* z^*) - 2\left(\frac{g_n^*}{2z^*}\right)^2 K_2(g_n^* z^*)\right] \quad (28)$$

$$E_{0\_specific}(z^*) = \frac{2\pi NC}{a_s^*} \sum_{p=0}^{\infty} \left(\frac{1}{2(z^* + p\Delta z^*)^2}\right) \quad (29)$$

$$E_{n\_specific}(z^*) = \frac{2\pi}{a_s^*}\left[C\left(\frac{g^*}{2z^*}\right) K_1(g_n^* z^*)\right] \quad (30)$$

where $\exp\left(-i\vec{g} \cdot \left[\overrightarrow{m_k} + \vec{\tau}\right]\right) = f_n(s_1, s_2)$ and the coefficient C is described as

$$C = (+ \text{ or } -)\left[\begin{array}{l} -2\left(\frac{1}{4\pi\varepsilon_0}\right)^2 \frac{\alpha q_B}{2r_1^4}\sqrt{q_B^2 2(1+\cos\varphi) + \frac{q_{Mg}^2}{d^4} + 2\frac{|q_B| q_{Mg}}{d^4}\sqrt{2(1+\cos\varphi)}\cos\theta} \\ -\left(\frac{1}{4\pi\varepsilon_0}\right)^2 \frac{2\alpha q_{Mg}}{2r_3^4}\sqrt{q_B^2 2d^4(1+\cos\varphi) + q_{Mg}^2 + 2d^2|q_B| q_{Mg}\sqrt{2(1+\cos\varphi)}\cos\theta} \end{array}\right]$$

In order to solve equation (26), we need an analytical representation of $f_n(s_1 s_2)$. Each pair of (s_1, s_2) along with other parameters provided in Table 1S (Supplementary Document), produces a trigonometric function of $f_n(s_1 s_2)$. The (s_1, s_2) - dependent terms in the energy equation (26) (E_n) were calculated for n up to 5. The isosteric heat of adsorption in the limit of zero coverage (referring to adsorption of the very first H_2 molecule on an ideal MgB_2 surface plane)[18] and the Henry's law constant can be expressed as below:

$$\lim_{n\to 0} \Delta H_{ads} = R \times \left(\frac{\partial(\ln K)}{\partial\left(\frac{1}{T}\right)} - T\right) \quad (31)$$

where ΔH_{ads} $(kJ\ mol^{-1})$ is the isosteric heat of adsorption in the limit of zero coverage, k $(m_2\text{kg}\ s^{-2}K^{-1})$ is the Boltzmann constant $T(K)$ is the temperature, $V(m^3)$is the gas space volume in the adsorption container, R $(atm.m^3K/mol)$ is the gas constant, K_H (nm) is the Henry's Law constant . In this scenario, there is no adsorbate-adsorbate lateral interaction, and the moles of adsorbed H_2 molecules (Gibbsian surface excess of a pure gas), n_a, is linearly dependent on equilibrium pressure (p)[42], leading to the calculation of Henry's law constant (K_H) as below:

$$K_H = \lim_{p\to 0}\left(\frac{n_a}{p}\right) \quad (32)$$

This Henry's law constant can also be theoretically calculated via interaction energy of an isolated molecule with a surface and later obtained to calculate the isosteric heat of adsorption at zero coverage, ΔH_{ads} (Clausius – Clapeyron equation)

$$K_H = \frac{1}{kT}\int_V [\exp\left(\frac{-u_s(r)}{kT}\right) - H(z-z_0)]\ dr \approx \frac{1}{kT}\int \quad (33)$$

$$\int_0^\infty \int_0^1 \int_0^1 \left[\exp\left(\frac{-\varepsilon_{gs} \times [E_{0_{non-specific}}(z^*) + E_{n_{non-}}}{}\right.\right.$$

$$+= \frac{1}{kT}\int_0^\infty \exp\left(\frac{-E_0(z^*)}{kT}\right)\int_0^1\int_0^1\left[exp\left(\frac{-\sum_{n=1}^{5} I}{}\right.\right.$$

where $E_0, E_n\ (n = 1-5)$ are functions of z^* only and thus independent of s_1,s_2, so E_0 can be extracted from the double integral of s_1,s_2; $f_n\ (n = 1-5)$ are trigonometric functions of s_1,s_2; H is the Heaviside function and z_0 is the distance value at which the total interaction energy has a value of zero. MATLAB was used to find a fit equation for $ln(K_H)$ and $1/T$.

Computational method

Plane-wave, periodic supercell DFT calculations were performed with the Vienna *ab initio* simulation package (VASP), version 5.4.4,[43] using the projector augmented wave treatment of core−valence interactions[44,45] with the SCAN (Strongly Constrained and Appropriately Normed) functional with rVV10 vdW corrections.[46,47] The initial bulk structure of metal diborides was obtained from the Materials Project.[48] For all calculations, the energy cutoff for the plane-wave basis set was set to 400 eV, and self-consistent-field electronic energies were converged to 10^{-4} eV and atomic forces to <0.03 eV/Å. Five slab models were created from the bulk structure, including B-terminated (0001), Mg-terminated $(000\bar{1})$, B-terminated $(10\bar{1}0)$, Mg-terminated $(10\bar{1}0)$, and $(11\bar{2}0)$. Each slab was separated from periodic images by at least 15 Å of vacuum with monopole/dipole and quadrupole corrections applied perpendicular to the slab to the total energy to avoid undesired cross-cell interactions. The Brillouin zone was sampled with a Γ-centered 4 × 4 × 1 k-point mesh for (0001) slab structures, and a Γ-centered 1 × 3 x 3 k-point mesh for $(10\bar{1}0$ slab structures, and a Γ-centered 3 × 1 × 3 k-point mesh for $(11\bar{2}0)$ slab structures. Geometry optimization of the B-terminated $(10\bar{1}0)$ leads to extensive surface reorganization into an amorphous state suggesting that the surface energy of that plane is too high to be stabilized. POSCAR files of optimized structures are included in the Supplement Information. Bader charge analyses were performed using the algorithm developed by Henkelman *et al.*[38–41] For H_2 adsorption calculations, binding strength was quantified by referencing to gas phase H_2 following

$$E_{H_2ads} = E_{surface+H_2} - E_{surface} - E_{H_2}$$

where $E_{surface+H_2}$, $E_{surface}$ and E_{H_2} are DFT-computed energies of a surface with an adsorbed H_2, the adsorbate-free clean surface and H_2 in gas phase, respectively.

Result

Analytical Study: Interaction Energy

The fluctuating dipole (red, square), induced dipole (green) and total (blue, triangular) interaction energies of the five planes: B-terminated (0001), Mg-terminated $(000\bar{1})$, B-terminated $(10\bar{1}0)$, Mg-terminated $(10\bar{1}0)$, and Mg-B $(11\bar{2}0)$, over a reasonable range $(1-10$ Å$)$ of distances between H_2 and MgB_2 were plotted in Figure 5.

Generally, as the distance between two entities decreases, the fluctuating dipole and total interaction energies show increasing attraction (energy value goes more negative) to its depth and then rises to positive values which indicates increasing repulsion. From Figure 5, Mg (0001) has the smallest attractive energy $(\sim -5\ kJ\ mol^{-1})$ while the other 4 terminated planes have interaction energies falling in the range of $-15\ to\ -20\ kJ\ mol^{-1}$. Among the two basal planes (B (0001) and Mg $(000\bar{1})$), which are experimentally more often seen as terminated planes of MgB_2,[49–52] B-terminated (0001) showed higher affinity to H_2 molecules. Recalling equations 26 - 30, this interaction energy is dependent on the calculated charge values of the surface atoms and thus subjected to deviation. A detailed discussion of this effect is presented in the subsection below. Regarding the induced dipole interaction energy, it does not follow a trend. This energy depends on the total induced dipole direction (referring to discussion about Figure 5), which simultaneously creates attraction to one layer and repulsion to the other layer. At discreet distance and specified charge values, either repulsion force or attraction force prevails. Therefore, as the distance between two entities decreases, we witnessed a similar trend among the three lines in Figure 5 a,b,d,e; while in Figure 5 c and f, the induced dipole interaction energy was decreasing. By observing the proximity between the "green" - induced dipole and "blue, triangular"- total interaction energy lines in all 5 terminated planes, it can also be concluded that the total interaction energy is dominated by the induced dipole interaction energy. A similar conclusion was drawn from *Cygan et. al.* about molecular models for interaction with minerals, which claimed the dominance of Coulombic forces (induced dipole energy) over short-range repulsion, and attractive van der Waals, which both contribute to fluctuating dipole energy.[53] In Figure 5b at $x = 6.2$ Å, we observed a sharp change in total interaction energy. This results from the dipole

change at distance $x = 6.2$ Å and the analytical calculation were run in MATLAB software at discreet values of distance, leading to a discontinuity in the graph. This, however, does not change the physical nature of adsorption potential.

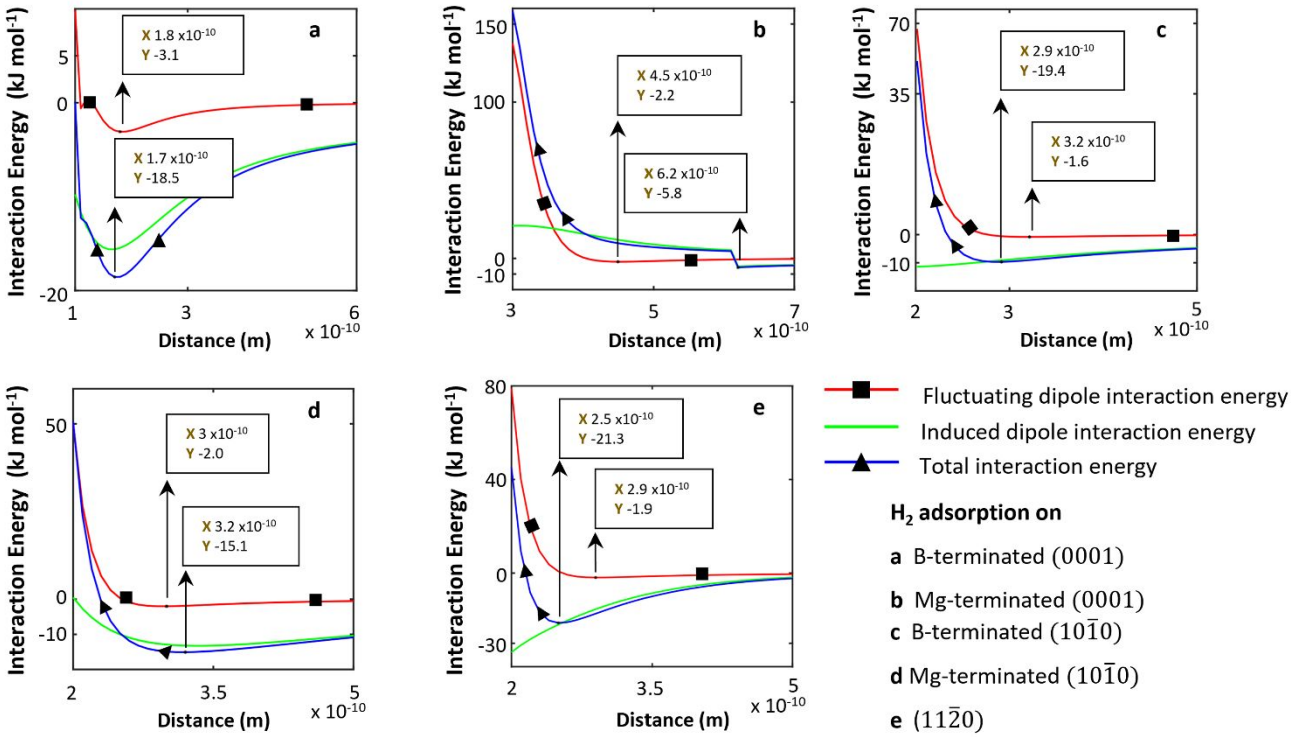

Figure 5: The interaction energies of H_2 molecule adsorption onto 5 types of MgB_2 surface exposed planes. The black boxes on the red and blue lines indicate distance X and energy value Y of the potential well depth of fluctuating dipole energy and total interaction energy respectively.

Analytical Study: Dependence on charge. The total interaction energy, as described in equations (26) – (30), is a function of charge values. The charge values used as inputs to the analytical model were found using DFT-computed Bader charge approximation, with an acceptable deviation (σ) of $\pm$ 0.2 depending on the functional used. The interaction energies of the 5 planes were mapped out as Mg and B charges deviate $\pm$ 0.2 e from their calculated values. A table of interaction energies at different charge values is presented in Supplementary Document – Table 2S. As we can see from Figure 6, the interaction energy varies significantly within the range of charge deviation $[-0.2, 0.2]$, in which the strongest interaction energy can be twice as large as the weakest one. Previous studies have shown that, in hydrogen physisorption on metal-doped structures and metallic frameworks, interaction energy does not exceed $30\ kJ\ mol^{-1}$.[54–57] Adsorption on pure carbon-based structures can have even lower interaction energies, as discussed in the introduction. Therefore, as we vary the charge values, all interaction energy that exceeded $30\ kJ\ mol^{-1}$ should be considered with caution. Examining the results in Figure 6, we again confirm the possibility of manipulating surface charge to change adsorption energy. This is another avenue for engineering in materials research for applications of separations or energy storage, in which the arduous quest for new materials or chemical modifications may be supplanted with tunability of surface charge. The integrated effect of van der Waals and electrostatic attraction present in layered materials' intra- and inter-layer interactions have been significantly studied recently, demonstrating that the calculation of surface charge cannot be omitted.[58,59] The intercalation process, which is enabled in layered materials, can potentially weaken the intralayer interaction by disturbing the electron sharing between Mg and B atoms, thereby easing delamination.[60]

Analytical Study: Isosteric Heat of Adsorption

Calculation of the the Henry's law constant enabled fitting to a linear function: $(K_H) = a \times \left(\frac{1}{T}\right) + b$ with a and b defined as constants for the 5 various terminated planes. Increasing $ln(K)$ with increasing reciprocal temperature implies positive values of the constant a. As introduced by Steele, equation (19) can be written as: $K_H = \frac{1}{kT} \int_V [exp\left(\frac{-u_s(r)}{kT}\right) - 1]\, dr$ using absolute void volume; this leads to negative values of the Henry's law constant.[33] Do *et al.* later adjusted this equation, as shown in equation (33), by considering accessible volume, resulting in positive values of the Henry's law constant.[61] Recalling equation (31) for isosteric heat of adsorption, with positive constant a, we should expect a trend of decreasing q_{st} values with increasing temperature. Table 2 – column 2 presents the isosteric heat of adsorption at zero coverage for hydrogen adsorption on 5 terminated planes at varying temperatures. The q_{st} values of each terminated plane all have magnitudes in the small range of $1 - 4\ kJ\ mol^{-1}$. With a very small coefficient for temperature (T), we can conclude that at the limit of 0 K, isosteric heat of adsorption is independent of temperature.

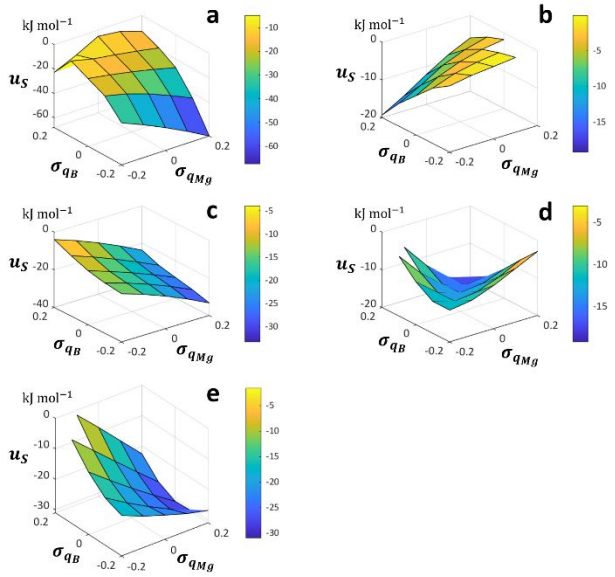

Figure 6: Surface plots illustrating the interaction energy (u_s) sensitivity to the change in charge values of Mg and B by $\pm$ 0.2 with (σ_{Mg},σ_B). (a) B-terminated (0001) plane (b) Mg-terminated (0001) plane (c) B $(10\bar{1}0)$ (d) Mg $(10\bar{1}0)$ plane (e) the $(11\bar{2}0)$ plane.

First-principles Study

The first-principles DFT study calculated the binding strength of H_2 to various MgB_2 terminated planes. The results are reported in the third column of Table 2. Binding of H_2 on B (0001) showed the strongest interaction, with $-6.3\ kJ\ mol^{-1}$. There appears to be no significant difference in binding energies on other terminated planes, approximately $-3\ kJ\ mol^{-1}$.

Even though the analytical interaction energies fall in the desired range ($\sim 15-48\ kJ\ mol^{-1}$),[26] both isosteric heat of adsorption and first-principles binding energy calculations show low values (physisorption) between one gaseous H_2 molecule and all 5 studied terminated planes of MgB_2. Considering these results in light of the high storage capacity that was experimentally witnessed on MgB_2, we lean towards the postulate that H_2 dissociates subsequent to adsorption, followed by H atoms' diffusion into the crystal lattice.[3–6] Noticeably, all of these energies fall within the range of interaction energies (Table 2 - column 4), which change with the deviation of charges. Even though there is variation between the analytical and computational results, the $2-3\ kJ\ mol^{-1}$ difference between analytical isosteric heat of adsorption and first-principles binding energy is insignificant. Based on this result, there is no distinct preference of the H_2 molecule among the different terminated planes of MgB_2. We examined the $(11\bar{2}0)$ plane, which has not been well studied, and even this plane shows similar interaction energy to other planes.

Table 2: Isosteric heat of adsorption at zero coverage of the 5 terminated planes.

Plane	Isosteric Heat of Adsorption ($kJ\ mol^{-1}$)	First-principles study energy ($kJ\ mol^{-1}$)	Analytical Interaction Energy ($kJ\ mol^{-1}$)		
			Energy at depth in Figure 5 *	Max. value **	Min. value **
$B\ (0001)$	1.8 $-0.0083\times T+1.816$	-6.3	-18.5	-67.6	-4.9
$Mg\ (0001)$	1.9 $-0.0083\times T+1.9047$	-3.1	-5.8	-19.3	-0.1
$B\ (10\bar{1}0)$	1.3 $-0.0083\times T+1.291$	-3.8	-19.4	-33.3	-3.8
$Mg\ (10\bar{1}0)$	1.25 $-0.0083\times T+1.26$	-3.8	-15.1	-19.1	-2.9
$(11\bar{2}0)$	3.35 $-0.0083\times T+3.63$	-3.0	-21.3	-31	-1.6

*This is the lowest point in the total interaction energy curve (blue, rectangular line) in Figure 5. **These are the maximal and minimal magnitudes of (*) when charges of Mg and B are varied $\pm$ 0.2 e

Conclusions

An analytical model was formulated to examine the interaction energy of a singular nonpolar H_2 molecule physisorbed on MgB_2 material surfaces. A first-principles DFT study was able to calculate the surface charges of Mg and B on each terminated plane, which provided input to the analytical calculations. This analytical study incorporates both van der Waals and electrostatic interactions. Because MgB_2 is a layered material, charges of Mg and B are not the same between the terminated, exposed plane and its direct sublayer/sublayers. Mg-terminated (0001) was analytically found to have the weakest interaction energy($-5.8\ kJ\ mol^{-1}$) , while the values for remaining four planes range from -15 to $-20\ kJ\ mol^{-1}$. We also witnessed that a dipole flipping phenomenon emerged from the analytical study, in the approach of an H_2 molecule to the Mg-terminated (0001) surface. The isosteric heat of adsorption values at zero coverage of these terminated planes do not differ significantly from each other ($1-4\ kJ\ mol^{-1}$). Computational results also showed low binding energies with the strongest one being $-6.3\ kJ\ mol^{-1}$ for $B\ (0001)$. The low interaction energies between molecular H_2 and MgB_2 planes suggest that another subsequent chemical step exists, or extreme reaction condition is required for the previous observation of high hydrogen storage in MgB_2. The formulation exhibits a significant dependence of interaction energy on surface charges and is able to offer an analytical representation for gas adsorption on solid surfaces, or more specifically, gaseous molecule adsorption on a layered, metallic sorbent.

Author Contributions

Thi Kieu Ngan Pham: data curation, formal analysis, investigation, methodology, visualization, writing. Sichi Li: data curation, formal analysis, funding acquisition, methodology, software, validation. Joseph J. Brown: conceptualization, funding acquisition, methodology, project administration, supervision, validation, writing - review & editing.

Conflicts of interest

There are no conflicts to declare.

Acknowledgements

The paper is funded by Department of Energy EPSCOR grant: DE-SC0020213 Fostering a Guided Multiscale Model for the Development of Advanced MgB_2 Hydrogen Storage Materials. SL acknowledges financial support through the Hydrogen Storage Materials Advanced Research Consortium (HyMARC) of the U.S. Department of Energy (DOE), Office of Energy Efficiency and Renewable Energy, Fuel Cell Technologies Office under Contract DE-AC52-07NA27344. A portion of the work was performed under the auspices of the DOE by Lawrence Livermore National Laboratory (LLNL) under Contract DE-AC52-07NA27344. The authors appreciate useful discussions with Dr. Rui Sun and Dr. Craig Jensen at the Department of Chemistry, University of Hawai'i at Mānoa and with Dr. Channing C. Ahn at the California Institute of Technology.

References

1 DOE Establishes Bipartisan Infrastructure Law's $9.5 Billion Clean Hydrogen Initiatives, https://www.energy.gov/articles/doe-establishes-bipartisan-infrastructure-laws-95-billion-clean-hydrogen-initiatives, (accessed Oct 10 2022).

2 S. Satyapal, J. Petrovic, C. Read, G. Thomas and G. Ordaz, The U.S. Department of Energy's National Hydrogen Storage Project: Progress towards meeting hydrogen-powered vehicle requirements, *Catal. Today*, 2007, **120**, 246–256.

3 Y. Nakamori and S. Orimo, in *Solid-state hydrogen storage*, Elsevier, 2008, pp. 420–449.

4 Y. Filinchuk, B. Richter, T. R. Jensen, V. Dmitriev, D. Chernyshov and H. Hagemann, Porous and Dense Magnesium Borohydride Frameworks: Synthesis, Stability, and Reversible Absorption of Guest Species, *Angew. Chem., Int. Ed.*, 2011, **50**, 11162–11166.

5 M. J. van Setten, G. A. de Wijs, M. Fichtner and G. Brocks, A density functional study of α-Mg $(BH_4)_2$, *Chem. Mater.,*2008, **20**, 4952–4956.

6 G. Severa, E. Rönnebro and C. M. Jensen, Direct hydrogenation of magnesium boride to magnesium borohydride: demonstration of >11 weight percent reversible hydrogenstorage, *Chem. Commun.*, 2010, **46**, 421–423.

7 K.-H. Jin, H. Huang, J.-W. Mei, Z. Liu, L.-K. Lim and F. Liu, Topological superconducting phase in high-Tc superconductor MgB2 with Dirac–nodal-line fermions, *npj Comput. Mater.*, 2019, **5**, 57.

8 M. E. Jones and R. E. Marsh, The Preparation and Structure of Magnesium Boride, MgB_2, *J. Am. Chem. Soc.*, 1954, **76**, 1434–1436.

9 D. R. Armstrong and P. G. Perkins, Electronic band structure of magnesium diboride*, J. Chem. Soc., Faraday Transactions 2: Molecular and Chemical Physics*, 1979, **75**, 12–16.

10 G. J. Kubas, Fundamentals of H_2 Binding and Reactivity on Transition Metals Underlying Hydrogenase Function and H_2 Production and Storage, https://pubs.acs.org/doi/pdf/10.1021/cr050197j, (accessed October 10, 2022).

11 N. Park, S. Hong, G. Kim and S.-H. Jhi, Computational Study of Hydrogen Storage Characteristics of Covalent-Bonded Graphenes, *J. Am. Chem. Soc.*, 2007, **129**, 8999–9003.

12 P. Chen, X. Wu, J. Lin and K. L. Tan, High H_2 uptake by alkali-doped carbon nanotubes under ambient pressure and moderate temperatures, *Science*, 1999, **285**, 91–93.

13 B. M. W. Trapnell, The activities of evaporated metal films in gas chemisorption, *Proc. R. Soc. London, Ser. A*, 1953, **218**, 566–577.

14 S. J. Holden and D. R. Rossington, Hydrogen adsorption on silver, gold, and aluminum. Studies of parahydrogen conversion, J*. Phys. Chem.*, 1964, **68**, 1061–1067.

15 P. S. Rudman, Hydriding and dehydriding kinetics, *J. Less-Common Met.*, 1983, **89**, 93–110.

16 G. Sandrock, A panoramic overview of hydrogen storage alloys from a gas reaction point of view, *J. Alloys Compd.,*1999, **293**, 877–888.

17 Q. Lai, M. Paskevicius, D. A. Sheppard, C. E. Buckley, A. W. Thornton, M. R. Hill, Q. Gu, J. Mao, Z. Huang, H. K. Liu, Z. Guo, A. Banerjee, S. Chakraborty, R. Ahuja and K.-F. Aguey-Zinsou, Hydrogen Storage Materials for Mobile and Stationary Applications: Current State of the Art, *ChemSusChem*, 2015, **8**, 2789–2825.

18 K. Christmann, Interaction of hydrogen with solid surfaces, *Surf. Sci. Rep.*, 1988, **9**, 1–163.

19 J. K. Nørskov, A. Houmøller, P. K. Johansson and B. I. Lundqvist, Adsorption and Dissociation of H 2 on Mg Surfaces, *Phys. Rev. Lett.*, 1981, **46**, 257–260.

20 H. Nakatsuji and M. Hada, Interaction of a hydrogen molecule with palladium, *J. Am. Chem. Soc.*, 1985, **107**, 8264–8266.

21 K. G. Ray, L. E. Klebanoff, J. R. I. Lee, V. Stavila, T. W. Heo, P. Shea, A. A. Baker, S. Kang, M. Bagge-Hansen, Y.-S. Liu, J. L. White and B. C. Wood, Elucidating the mechanism of MgB_2 initial hydrogenation via a combined experimental–theoretical study, *Phys. Chem. Chem. Phys.*, 2017, **19**, 22646–22658.

22 Y.-S. Liu, K. G. Ray, M. Jørgensen, T. M. Mattox, D. F. Cowgill, H. V. Eshelman, A. M. Sawvel, J. L. Snider, W. York and P. Wijeratne, Nanoscale Mg–B via Surfactant Ball Milling of MgB_2: Morphology, composition, and improved hydrogen storage properties, *. Phys. Chem. C*, 2020, **124**, 21761–21771.

23 S. Jeong, T. W. Heo, J. Oktawiec, R. Shi, S. Kang, J. L. White, A. Schneemann, E. W. Zaia, L. F. Wan, K. G. Ray, Y.-S. Liu, V. Stavila, J. Guo, J. R. Long, B. C. Wood and J. J. Urban, A Mechanistic Analysis of Phase Evolution and Hydrogen Storage Behavior in Nanocrystalline $Mg(BH_4)_2$ within Reduced Graphene Oxide, *ACS Nano*, 2020, **14**, 1745–1756.

24 H.-W. Li, K. Kikuchi, Y. Nakamori, N. Ohba, K. Miwa, S. Towata and S. Orimo, Dehydriding and rehydriding processes of well-crystallized $Mg(BH_4)_2$ accompanying with formation of intermediate compounds, *Acta Mater.*, 2008, **56**, 1342–1347.

25 E. Rönnebro and E. H. Majzoub, Calcium borohydride for hydrogen storage: catalysis and reversibility, *J. Phys. Chem. B*, 2007, **111**, 12045–12047.

26 G. I. Prayogo, H. Shin, A. Benali, R. Maezono and K. Hongo, Importance of Van der Waals Interactions in Hydrogen

Adsorption on a Silicon-carbide Nanotube Revisited with vdW-DFT and Quantum Monte Carlo, *ACS Omega*, 2021, **6**, 24630–24636.

27 M. R. Mananghaya, A simulation of hydrogen adsorption/desorption in metal-functionalized BN nanotube, *Mater. Chem. Phys.*, 2020, **240**, 122159.

28 B. C. Wood, T. W. Heo, S. Kang, L. F. Wan and S. Li, Beyond Idealized Models of Nanoscale Metal Hydrides for Hydrogen Storage, *Ind. Eng. Chem. Res.*, 2020, **59**, 5786–5796.

29 M. S. Dresselhaus, Intercalation In Layered Materials, *MRS Bull.*, 1987, **12**, 24–28.

30 A.Talapatra, S. K. Bandyopadhyay, P. Sen, P. Barat, S. Mukherjee and M. Mukherjee, X-ray photoelectron spectroscopy studies of MgB_2 for valence state of Mg, *Phys. C: Supercond. Appl.*, 2005, **419**, 141–147.

31 S. Y. Wu, P.-H. Shih, J.-Y. Ji, T.-S. Chan and C. C. Yang, Direct observation of charge re-distribution in a MgB_2 superconductor, *Supercond. Sci. Technol.*, 2016, **29**, 045001.

32 Y. Zhao, C. Ban, Q. Xu, S.-H. Wei and A. C. Dillon, Charge-driven structural transformation and valence versatility of boron sheets in magnesium borides, *Phys. Rev. B*, 2011, **83**, 035406.

33 W. A. Steele, The physical interaction of gases with crystalline solids: I. Gas-solid energies and properties of isolated adsorbed atoms, *Surf. Sci.*, 1973, **36**, 317–352.

34 P. Modi and K.-F. Aguey-Zinsou, Room Temperature Metal Hydrides for Stationary and Heat Storage Applications: A Review, *Front. Energy Res.*, 2021, **9**, 128.

35 S. Li, H. Gunda, K. Ray, C.-S. Wong, P. Xiao, R. Friddle, Y.-S. Liu, S. Kang, J. Sugar, R. Kolasinski, L. Wan, A. Baker, J. Lee, K. Jasuja, M. Allendorf, V. Stavila and B. Wood, *Spontaneous Dynamical Disordering of Borophenes in MgB_2 and Related Metal Borides*, *Nat. Commun.*, 2021.

36 D. Baowan and J. M. Hill, Nested boron nitride and carbon-boron nitride nanocones, *Micro Nano Lett.*, 2007, **2**, 46.

37 L.-C. Lin, K. Lee, L. Gagliardi, J. B. Neaton and B. Smit, Force-field development from electronic structure calculations with periodic boundary conditions: applications to gaseous adsorption and transport in metal–organic frameworks, *J. Chem. Theory Comput.*, 2014, **10**, 1477–1488.

38 W. Tang, E. Sanville and G. Henkelman, A grid-based Bader analysis algorithm without lattice bias, *J. Phys.: Condens. Matter*, 2009, **21**, 084204.

39 E. Sanville, S. D. Kenny, R. Smith and G. Henkelman, Improved grid-based algorithm for Bader charge allocation, *J. Comput. Chem.*, 2007, **28**, 899–908.

40 G. Henkelman, A. Arnaldsson and H. Jónsson, A fast and robust algorithm for Bader decomposition of charge density, *Comput. Mater. Sci.*, 2006, **36**, 354–360.

41 M. Yu and D. R. Trinkle, Accurate and efficient algorithm for Bader charge integration, *J. Chem. Phys.*, 2011, **134**, 064111.

42 S. Sircar and D. V. Cao, Heat of Adsorption, *Chemical Engineering & Technology*, 2002, **25**, 945–948.

43 G. Kresse and J. Furthmüller, Efficient iterative schemes for *ab initio* total-energy calculations using a plane-wave basis set, *Phys. Rev. B*, 1996, **54**, 11169–11186.

44 P. E. Blöchl, Projector augmented-wave method, *Phys. Rev. B*, 1994, **50**, 17953

45 G. Kresse and D. Joubert, From ultrasoft pseudopotentials to the projector augmented-wave method, *Phys. Rev. B*, 1999, **59**, 1758

46 J. P. Perdew, K. Burke and M. Ernzerhof, Generalized Gradient Approximation Made Simple, *Phys. Rev. Lett.*, 1996, **77**, 4.

47 H. Peng, Z.-H. Yang, J. P. Perdew and J. Sun, Versatile van der Waals Density Functional Based on a Meta-Generalized Gradient Approximation, *Phys. Rev. X,* 2016, 15.

48 A. Jain, S. P. Ong, G. Hautier, W. Chen, W. D. Richards, S. Dacek, S. Cholia, D. Gunter, D. Skinner, G. Ceder and K. A. Persson, Commentary: The Materials Project: A materials genome approach to accelerating materials innovation, *APL Mater.*, 2013, **1**, 011002.

49 R. Saraswat, A. L. James and K. Jasuja, High yield synthesis of boron-based nanosheets, *Adv. Appl. Ceram.*, 2019, **118**, 209–216.

50 S. K. Das, A. Bedar, A. Kannan and K. Jasuja, Aqueous dispersions of few-layer-thick chemically modified magnesium diboride nanosheets by ultrasonication assisted exfoliation, *Sci. Rep.*, 2015, **5**, 10522.

51 S. K. Das and K. Jasuja, Chemical Exfoliation of Layered Magnesium Diboride To Yield Functionalized Nanosheets and Nanoaccordions for Potential Flame Retardant Applications, *ACS Appl. Nano Mater.*, 2018, **1**, 1612–1622.

52 Y.-U. Heo, S. Yoon, J. H. Kim, Y.-K. Kim, M. Kim, T.-J. Song, M. Maeda and S. X. Dou, Preferential growth of boron layer in magnesium diboride (MgB_2) by Mg diffusion method, *J. Alloys Compd.,*2017, **725**, 526–535.

53 R. T. Cygan, K. L. Nagy, P. V. Brady and E. A. Jenne, Molecular models of cesium sorption on kaolinite, *Adsorption of Metals by Geomedia, Academic Press, New York*, 1998, 383–399.

54 E. Tylianakis, G. M. Psofogiannakis and G. E. Froudakis, Li-Doped Pillared Graphene Oxide: A Graphene-Based Nanostructured Material for Hydrogen Storage, *J. Phys. Chem. Lett.*, 2010, **1**, 2459–2464.

55 E. Tsivion, J. R. Long and M. Head-Gordon, Hydrogen Physisorption on Metal–Organic Framework Linkers and Metalated Linkers: A Computational Study of the Factors That Control Binding Strength, *J. Am. Chem. Soc.*, 2014, **136**, 17827–17835.

56 A. Reisi-Vanani and S. Mehrdoust, Effect of boron doping in sumanene frame toward hydrogen physisorption: A theoretical study, *Int. J. Hydrogen Energy*, 2016, **41**, 15254–15265.

57 F. Ding and B. I. Yakobson, Challenges in hydrogen adsorptions: from physisorption to chemisorption, *Front. Phys.*, 2011, **6**, 142–150.

58 Q. Zhang, Y. Wang, Z. W. Seh, Z. Fu, R. Zhang and Y. Cui, Understanding the Anchoring Effect of Two-Dimensional Layered Materials for Lithium–Sulfur Batteries, *Nano Lett.*, 2015, **15**, 3780–3786.

59 R. Wang, T. Wang, H. Zobeiri, D. Li and X. Wang, Energy and charge transport in 2D atomic layer materials: Raman-based characterization, *Nanomaterials*, 2020, **10**, 1807.

60 B. Z. Xu, C. A. Barrett, D. R. Sexton, J. Chen, K. L. More, Z. Gai and T. T. S. S. P. Beckman, PhD thesis, Washington State University, 2017.

61 D. D. Do, D. Nicholson and H. D. Do, On the Henry constant and isosteric heat at zero loading in gas phase adsorption, *J. Colloid Interface Sci.*, 2008, **324**, 15–24.